Journal of The Electrochemical Society, **154** (4) D215-D219 (2007)
0013-4651/2007/154(4)/D215/5/$20.00 © The Electrochemical Society

Amorphous Carbon Coated Silicon Nanotips Fabricated by MPCVD Using Anodic Aluminum Oxide as the Template

Te-Ming Chen,[a] Fu-Ming Pan,[a,z] Jui-Yi Hung,[a] L. Chang,[a] Shich-Chuan Wu,[b] and Chia-Fu Chen[a]

[a]*Department of Materials Science and Engineering, National Chiao-Tung University, Hsinchu 30050, Taiwan*
[b]*National Nano Device Laboratories, Hsinchu 30078, Taiwan*

We have used nanoporous anodic aluminum oxide (AAO) as a template to fabricate amorphous carbon (α-C) coated silicon nanotips by microwave plasma chemical vapor deposition (MPCVD). During the preparation of the well-ordered AAO pore channel array, an underlying TiN layer was anodically oxidized as well in the late stage of the AAO anodization, forming titanium oxide nanomasks for Si nanotip fabrication. The titanium oxide nanomasks were then used to transfer the arrangement pattern of the AAO pore channel array to the Si substrate by plasma etch in the MPCVD system and, therefore, a well-ordered Si nanotip array was produced. An α-C layer ~5 nm thick was in situ deposited on the Si nanotips during the MPCVD process. The α-C layer was rich in nanocrystalline graphitic carbons according to Raman and Auger electron spectroscopies. The nanocrystalline graphitic carbons in the coating and the sharp tip shape made the Si nanotip a good field emitter and a field enhancement factor of ~659 was obtained.
 [DOI: 10.1149/1.2436629]

Manuscript submitted September 26, 2006; revised manuscript received December 4, 2006.
Available electronically February 8, 2007.

Nanostructured cold cathode materials have attracted much attention for their potential use in field emission applications because they usually exhibit a low threshold field for electron field emission.[1-5] Among various materials considered appropriate for field emission applications, crystalline Si has long been used as the starting material to fabricate field emitters because of their excellent electronic and mechanical properties and well-developed process techniques. Si field emission arrays can be readily fabricated on silicon wafers using standard microfabrication techniques, such as micromachining and integrated circuit processes, but a photolithography process is required to fabricate field emitter arrays when conventional microfabrication methods are used and, therefore, the size and density of field emitters are limited by the optical resolution of the lithography tool. Thus, many nanofabrication methods using Si wafers to prepare nanoscaled field emitters without the photomasking process have recently been developed. She et al.,[5,6] Hsu et al.,[7] and Lo et al.[8] have prepared Si nanotips by plasma etching the Si substrate using in situ deposited SiC nanoclusters as the nanomask. Wang et al.[9] have fabricated α-carbon (α-C) coated Si nanotips from a porous silicon substrate in a hot filament chemical vapor deposition system. For both the SiC-capped or the α-carbon coated Si tip array, field emission properties were greatly enhanced as compared to the uncoated one. However, most previously reported Si nanotips did not show an ordered arrangement because the preparation methods did not provide a growth process regulating the arrangement of the nanotips. In this study, we used porous anodic aluminum oxide (AAO) as the template to fabricate titanium oxide nanopillars with a hexagonally close-packed (hcp) arrangement, which in turn was used as the mask to direct the formation of silicon nanotips on the Si substrate in a microwave plasma chemical vapor deposition (MPCVD) system. Amorphous carbon could be coated in situ on the Si nanotips during the nanotip formation using a gas mixture of CH_4 and H_2 as the plasma source. The field-emission characteristics of the α-carbon coated Si nanotips was also studied.

Experimental

Figure 1 illustrates the fabrication steps for the α-C coated Si nanotips. First, a TiN thin film 30 nm thick was sputter deposited on the 4 in. p-type Si(100) wafers with a resistivity of 15–25 Ω cm, followed by the deposition of an Al film 3 μm thick on the TiN layer by thermal evaporation. Anodic oxidation of the Al film was carried out in 0.3 M oxalic acid ($H_2C_2O_4$) at 25°C under a constant polarization voltage of 40 V. The underlying TiN film could be partially anodically oxidized when the Al anodization was completed, thereby forming TiO_x nanopillars under the bottom of AAO pore channels. The AAO layer was then removed by wet chemical etch in a solution of 6 wt % H_3PO_4 and 1.5 wt % CrO_3 at 60°C for 40 min. The TiO_x nanodots were then used as the nanomask for etching the TiN layer and the underlying Si substrate in an inductively coupled plasma reactive ion etch (ICP-RIE) system using the gas mixture of BCl_3 and Cl_2 as the plasma source. The RIE process was performed under the following working conditions: plasma power on the 4 in. substrate plate 400 W, substrate bias power 100 W, and working pressure 10 Torr with a flow rate of 35 sccm for both the BCl_3 and Cl_2 gases. Fabrication of α-C coated Si nanotips was then carried out in a microwave plasma CVD (MPCVD) system under the following working conditions: microwave power on the 1 in. substrate plate 300 W, bias power 200 W, working pressure 1 Torr, CH_4-H_2 ratio = 20:80 sccm, and deposition time 30 min. Surface morphology and microstructure of the nanotips were studied by scanning electron microscopy (SEM, JEOL JSM-6500F) and high-resolution transmission electron microscopy (HRTEM, JEOL FX-II 2010). The chemical composition of the thin films and nanotips was investigated by Auger electron spectroscopy (AES, Thermo VG 350). Raman spectroscopy (LABRAM HR) was used to study the allotropic form of the α-carbon layer. Field emission measurement was performed under a vacuum condition of ~5×10^{-6} Torr with a Kei-

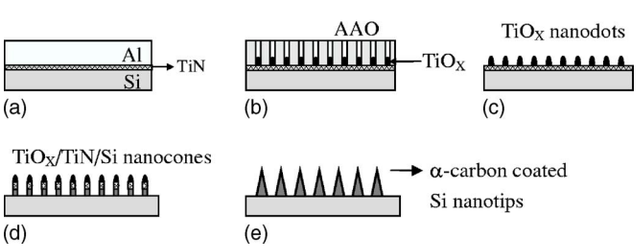

Figure 1. The fabrication steps of α-C coated Si nanotips: (a) TiN and Al deposited on the Si wafer by physical vapor deposition, (b) anodic oxidation of the Al film and formation of TiO_x nanomasks, (c) removal of the AAO layer by wet etch, (d) reactive ion etch of the remanent TiN and the Si substrate, and (e) Si nanotip formation by plasma etch and in situ deposition of the α-C layer on the nanotips during the MPCVD process.

[z] E-mail: fmpan@faculty.nctu.edu.tw

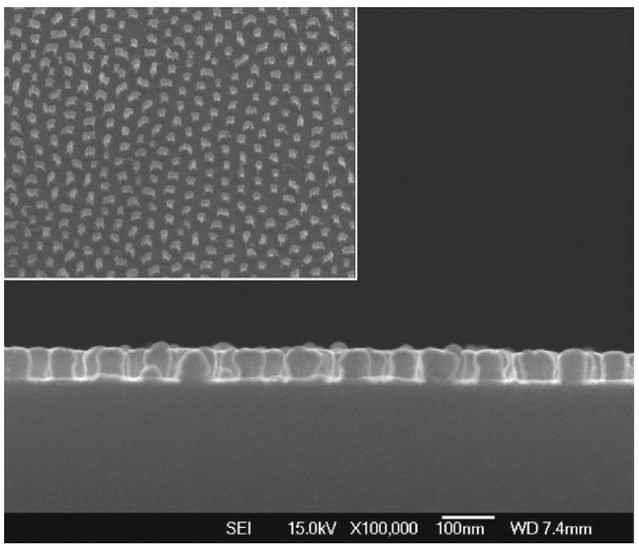

Figure 2. Cross-sectional SEM image of the TiO_x nanopillars after the removal of the AAO layer by wet etch. The inset shows the plane-view SEM image of the TiO_x nanopillar array.

thley 237 source measurement unit. The distance between the Si nanotip array and the cylindrical anode 2 mm in diameter was ~100 μm.

Results and Discussion

The nanoporous AAO template, which consisted of highly ordered pore channels with a uniform pore size of 70–80 nm and a pore-to-pore distance about 100 nm, was obtained under the anodic oxidation condition described above. In the late stage of the aluminum anodization, the underlying TiN film could also be anodically oxidized as the interface between the electrolyte and the AAO barrier layer approached the TiN area adjacent to the pore bottom.[10] The O^{2-}/OH^- ions in the electrolyte solution could diffuse through the thin AAO barrier layer, initiating anodic oxidation of the TiN layer, and thereby titanium oxide nanoparticles were formed under the AAO pore channels. Because the anodic oxidation was accompanied with volume expansion, the TiO_x particles protruded out of the TiN layer and grew into a pillar shape. The as-prepared nanopillars were basically amorphous titanium oxide according to our previous study.[11] Figure 2 shows the cross-sectional SEM image of the TiO_x nanopillars after removal of the AAO layer by wet etch. The TiO_x nanopillars were ~70 nm in height, and, like the AAO template, had a well-ordered hexagonal arrangement, as shown in the inset of Fig. 2. Since the TiO_x nanopillars were only formed under the AAO pore bottom, the remaining TiN needed to be removed before we could use the TiO_x pillars as the hardmask to fabricate Si nanotips. To etch the TiN layer, we used a gas mixture of BCl_3 and Cl_2 as the plasma source in the ICP-RIE system. TiO_x and Si could also be etched by the chorine-based plasma source, but the relatively large height of the TiO_x nanopillars provided sufficient masking thickness to the underlying TiN and Si substrate so that the arrangement pattern of the nanopillars could be successfully transferred to the Si substrate. The RIE etch led to the formation of a well-ordered nanocone structure with TiO_x and TiN on the apex and Si at the lower portion of the nanocone. Figure 3 shows a side-view SEM image of the nanocone array after the RIE etch for 55 s. The nanocone array had a hexagonal arrangement as the TiO_x nanomask. From the SEM image, some nanocones exhibited a less regular cone shape, and the remanent TiO_x/TiN nanomasks were not very uniform in size. This was because pattern transfer from those irregular

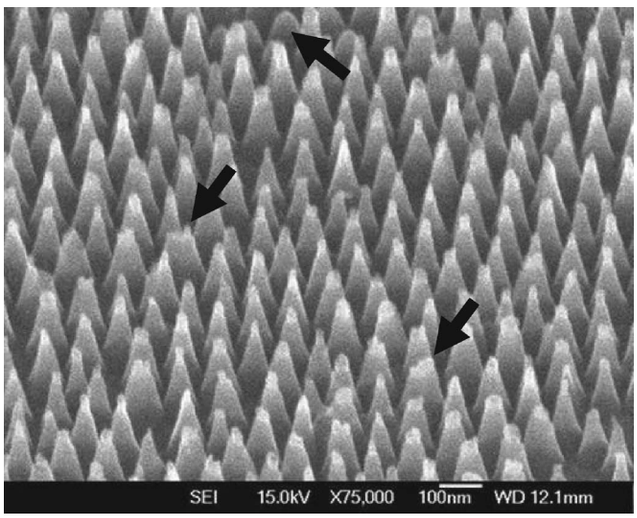

Figure 3. Side-view SEM image of the TiO_x/TiN/Si nanocone array after the RIE etch for 55 s.

TiO_x nanopillars, which were formed under the AAO pore channels near domain boundaries of the AAO template layer, would produce nanocones with an irregular shape.[10]

After the RIE process, the thus prepared TiO_x/TiN/Si nanocones then received further plasma treatment in the MPCVD system using the gas mixture of H_2/CH_4 as the plasma source. During the plasma treatment, the residual TiO_x and TiN were completely removed and formation of sharp Si nanotips could be achieved by chemical erosion with hydrogen radicals and ion sputtering. Figure 4 shows the side-view SEM image of Si nanotips after the plasma treatment. The tip-to-tip distance of most Si nanotips shown in the SEM image was close to the AAO pore-to-pore distance, ~100 nm. According to electron diffraction study (inset), the nanotips consisted of crystalline silicon. These observations indicated that formation of the Si nanotips was a result of plasma etch of the Si substrate. The apex angle of most Si nanotips shown in the figure was ~13°. The angle could be tailored by varying the RIE time. With a longer RIE time, the size and thickness of the TiO_x/TiN nanomask became smaller, thereby leading to the formation of a sharper Si nanotip during the MPCVD process. The average aspect ratio of the Si nanotips, which

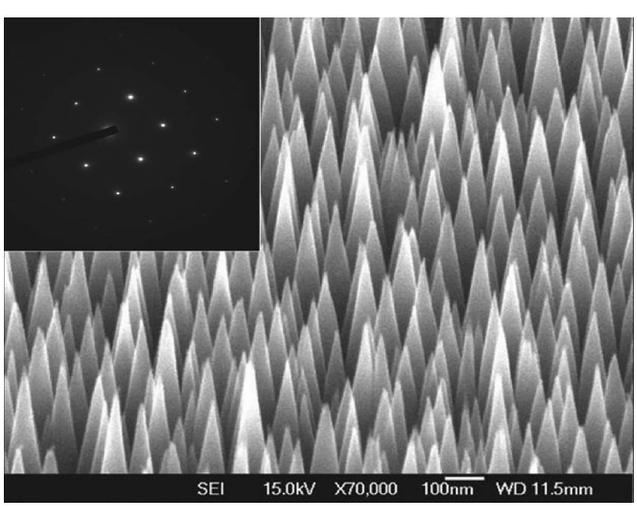

Figure 4. Side-view SEM image of Si nanotips after the MPCVD treatment. The inset is the electron diffraction pattern of the Si nanotips.

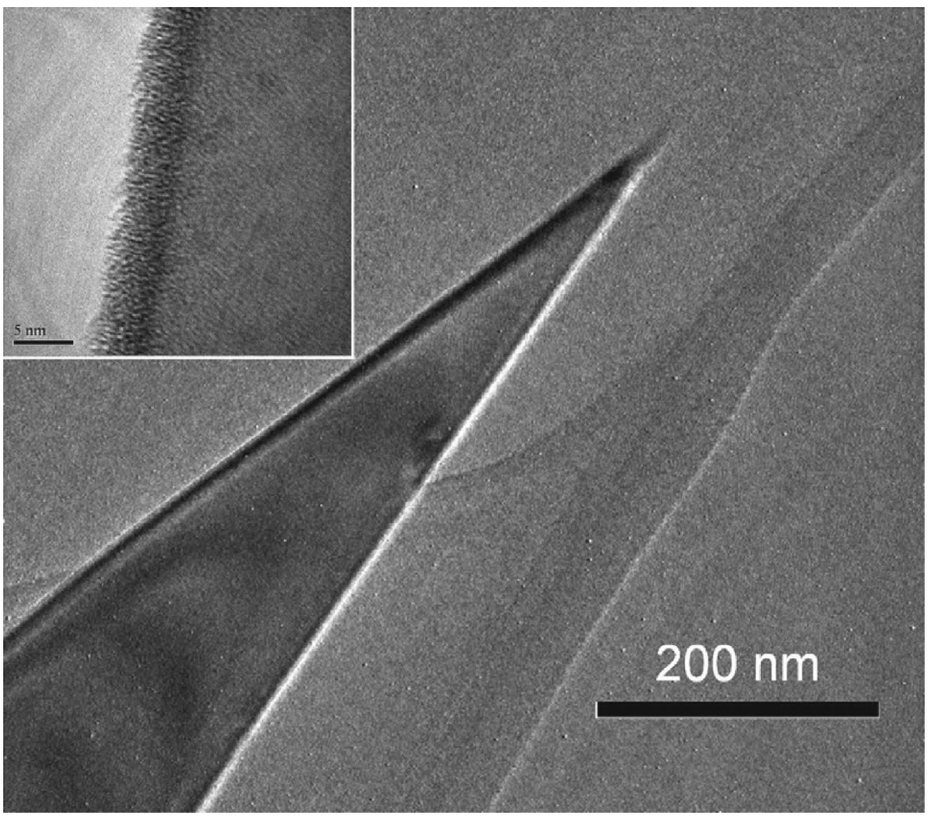

Figure 5. TEM image of a Si nanotip. The Si nanotip was coated by an amorphous layer with a thickness of ~5 nm, as shown in the inset.

was defined herein to be the ratio of the nanotip height to the diameter at the half height of the nanotips, was estimated to be ~6.5. Although the Si nanotip array had a rather ordered arrangement, it still seemed to be more random than that of the TiO_x nanomask array. In addition to the fact that irregular TiO_x nanomasks, such as those denoted in Fig. 3, could misshape the final geometric configuration of the Si nanotips, it was likely that some nanoclusters randomly scattered on the Si substrate could also play the masking role, leading to formation of additional Si nanotips. The origin of the nanoclusters could be either due to TiO_x/TiN nanomasks dislodged from the nanocones apex, or sputtered and/or redeposited silicon-containing clusters during the MPCVD process, as reported previously.[6]

During the etch of the Si substrate in the MPCVD system, an α-carbon layer could be in situ deposited on the Si nanotips. A TEM image of a Si nanotip, which was separated from the Si substrate by ultrasonic agitation, is shown in Fig. 5. The inset shows that the surface of the Si nanotip was coated by an amorphous layer with a thickness of ~5 nm. Electron energy loss spectroscopy (EELS) analysis for the Si nanotips showed that the amorphous layer was mainly composed of carbon. We used Raman spectroscopy and Auger spectroscopy to probe the chemical structure of the surface α-C layer on the nanotips. Figure 6 shows the Raman spectrum of the α-C coated Si nanotip array in the range of 1100–2000 cm^{-1}. Raman spectroscopy has been widely used to characterize the chemical structure of chemical-vapor-deposited carbon materials, such as diamond-like carbon (DLC) and carbon nanotubes.[12,13] Disordered graphitic carbon materials exhibit two major Raman peaks, G and D peaks, in the range of 1300–1700 cm^{-1},[13] and the two peaks are often used to characterize the sp^2 chemical bonding structure of CVD-deposited carbon materials. The D peak is commonly considered to be a ring breathing mode in a disordered graphitic structure and the G peak is due to sp^2 bond stretching. Peak features of both Raman modes, such as peak position and intensity, are greatly dependent on the sp^2 bonding structure of CVD deposited carbon materials. The G peak is particularly useful to reveal nanocrystallinity of the graphitic structure.[12] For a perfect and infinite graphite crystal, the D peak is absent in the Raman spectrum and the G peak situates at 1580 cm^{-1}. As the large graphite crystal disintegrates into nanocrystalline clusters, the G peak shift to a higher wavenumber and the D peak becomes prominent. The position of the G peak can be higher than 1600 cm^{-1} when the size of nanocrystalline graphite cluster is smaller than 2 nm.[13] In this work, the G and D peaks of the carbon overlayer appeared at ~1607 cm^{-1} and ~1335 cm^{-1}, respectively. The peak position of the G mode and a large intensity ratio of the D peak to G peak implied that a significant amount of nanosized graphitic structures were likely present in the carbon

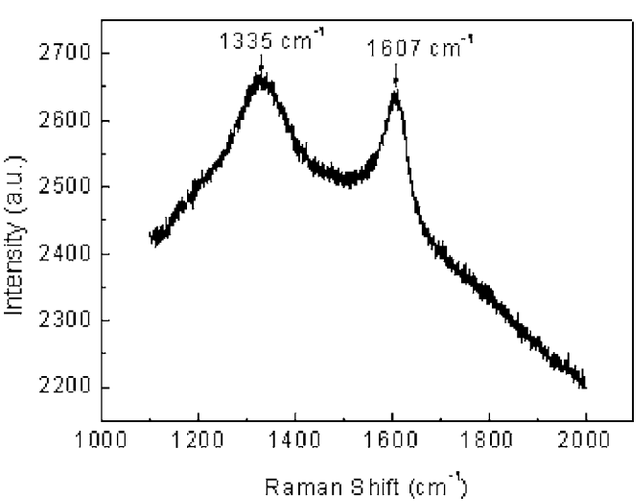

Figure 6. The Raman spectrum of the α-C coated Si nanotip array.

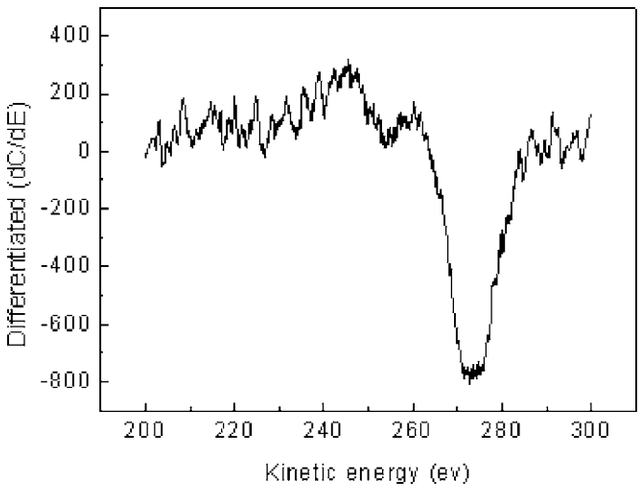

Figure 7. C(KVV) Auger electron spectrum of the α-C coated Si nanotip array.

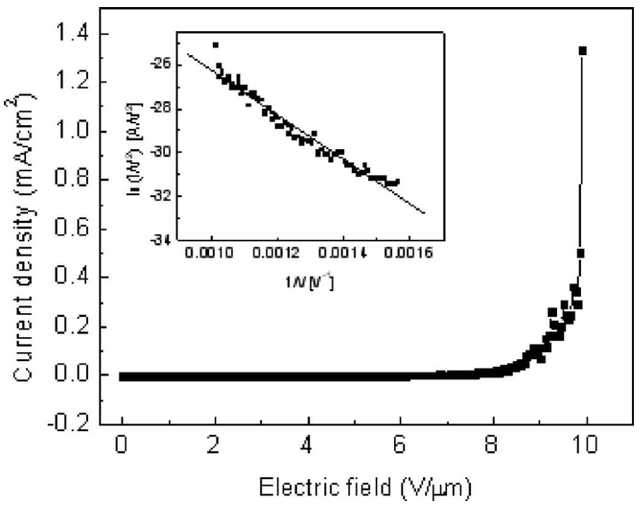

Figure 8. The *J-E* curve and the F–N plot (inset) for the α-C coated Si nanotip array.

layer. In addition, Auger study also suggested the deposition of graphitic carbon on the Si nanotips. Figure 7 is a differential C(KVV) Auger electron spectrum in the energy range of 200–300 eV for the amorphous carbon coated Si nanotips. Because valence electrons are involved in the C(KVV) Auger transitions, the peak position and line shape of the C(KVV) series are significantly affected by the chemical bonding structure of carbon atoms and, therefore, are often used to qualitatively characterize the allotropic form of carbon. The peaks at ~259 and ~246 eV are due to the $C(KV_1V_1)$ transition and the $C(KV_2V_1)$ transition, respectively.[14,15] The Auger line shape demonstrated a chemical structure with more characteristics of graphitic carbon, suggesting that the thin carbon layer was rich in graphitic bondings. This was consistent with the Raman spectroscopy study described above. The presence of nanocrystalline graphitic structure in the carbon layer on the Si nanotip array provided an electrically conductive path for electrons to the Si nanotip apex, thereby leading to a lower turn-on voltage for the field emission. Otherwise, the relatively high resistivity of the Si substrate from which the Si nanocones were fabricated would have had retarded the electron conduction, and thus the field-emission performance.

The sharp Si nanotips could greatly enhance the local field at the tip apex, and thereby dramatically improve the field emission property. The dependence of the emission current density of a field emitter on the applied field obeys the Fowler–Nordheim (F–N) relation[16]

$$I = aV^2 \exp(-b/V) \quad [1]$$

where V is the applied voltage, and a and b, under a practical measurement condition, are constants. In general, b equals $Bd\varphi^{3/2}/\beta$, where ϕ is the local work function of the emitter tip, d the separation between the emitter and the anode, B a constant ($=6.53 \times 10^7$ V eV$^{-3/2}$ cm^{-1}), and β the enhancement factor. β correlates the applied voltage V with the local electric field E_{loc} at the emitting surface by the relation $E_{loc} = \beta(V/d)$. β is closely related to the geometric shape of the field emitter and can be approximated by

$$\beta = \frac{d}{kr(d-r)} \quad [2]$$

where r is the radius of curvature of the tip, and k is a constant depending on the tip geometry.[17] For a simple diode measurement configuration, d is usually much larger than r, i.e., $d \gg r$, and thus β can be approximated as $1/kr$. This suggests that emitters with a sharper tip have better field emission characteristics due to the larger β value. Figure 8 shows the field emission current density (J) of the α-C coated Si nanotip array as a function of the electric field (E). The F–N plot derived from the *J–E* curve is shown in the inset. The field enhancement factor of a field emitter can be estimated from the slope of the F–N plot, which equals $-Bd\varphi^{3/2}/\beta$. The slope of the F–N plot in Fig. 8 was −10,222, and the β value of the Si nanotip was thus calculated to be 659, assuming a work function of graphite, 4.6 eV.[18] The relatively large β value, compared to some previously reported values for Si nanowires, e.g., β = 455 in Ref. 5, could be attributed to the sharp tip apex and high aspect ratio of the Si nanotips. Combined with the nanocrystalline graphitic structure of the α-C coating layer, which had a higher electrical conductivity and a lower work function than crystalline silicon, the very sharp tip shape significantly improved the field emission property of the Si nanotip array.

Conclusion

We have successfully fabricated α-C coated silicon nanotips by MPCVD using nanoporous AAO as a template. The Si nanotips were produced by plasma etch and the α-C layer was in situ deposited on the nanotips under the MPCVD process conditions. During the plasma etch, the Si substrate was masked by the well-ordered TiO_x nanopillar array, which was formed under the bottom of AAO pore channels and thus had a close-packed hexagonal arrangement as the AAO pore channel array. The TiO_x nanomasks transferred the hexagonal arrangement pattern to the Si substrate, leading to the formation of the well-ordered Si nanotip array. The in situ deposited α-C layer on the Si nanotip was rich in nanocrystalline graphitic carbons according to Raman and Auger electron spectroscopies. Due to the sharp geometric feature, the Si nanotip had a large field enhancement factor of 659 and, therefore, exhibited a good field emission performance.

Acknowledgments

This work was supported by the National Science Council of China, under contract no. NSC93-2120-M-009-007. Technical support from the National Nano Device Laboratories (NDL) is gratefully acknowledged.

National Chiao Tung University assisted in meeting the publication costs of this article.

References

1. P.-L. Chen, J.-K. Chang, C. T. Kuo, and F.-M. Pan, *Diamond Relat. Mater.,* **13**, 1949 (2004).
2. O. L. Golubev, T. I. Sudakova, and V. N. Shrednik, *Tech. Phys.,* **45**, 1575 (2000).
3. R. Z. Bakhtizin, S. S. Ghots, and E. K. Ratnikova, *IEEE Trans. Electron Devices,* **38**, 2398 (1991).

4. S. H. Ahn, K. R. Lee, K. Y. Eun, and D. Jeon, *Surf. Coat. Technol.,* **120–121**, 734 (1999).
5. J. C. She, S. Z. Deng, N. S. Xu, R. H. Yao, and J. Chen, *Appl. Phys. Lett.,* **88**, 013112 (2006).
6. J. C. She, K. Zhao, S. Z. Deng, J. Chen, and N. S. Xu, *Appl. Phys. Lett.,* **87**, 052105 (2005).
7. C. H. Hsu, H. C. Lo, C. F. Chen, C. T. Wu, J. S. Hwang, D. Das, J. Tsai, L. C. Chen, and K. H. Chen, *Nano Lett.,* **4**, 471 (2004).
8. H. C. Lo, J. S. Hwang, K. H. Chen, C. H. Hsu, C. F. Chen, and L. C. Chen, *Appl. Phys. Lett.,* **83**, 1420 (2003).
9. Q. Wang, J. J. Li, Y. J. Ma, X. D. Bai, Z. L. Wang, P. Xu, C. Y. Shi, B. G. Quan, S. L. Yue, and C. Z. Gu, *Nanotechnology,* **16**, 2919 (2005).
10. P.-L. Chen, C. T. Kuo, T.-G. Tsai, B.-W. Wu, C. C. Hsu, and F.-M. Pan, *Appl. Phys. Lett.,* **82**, 2796 (2003).
11. P.-L. Chen, C. T. Kuo, and F.-M. Pan, *Appl. Phys. Lett.,* **84**, 3888 (2004).
12. M. A. Tamor and W. C. Vassell, *J. Appl. Phys.,* **76**, 3823 (1994).
13. A. C. Ferrari and J. Robertson, *Phys. Rev. B,* **61**, 14095 (2000).
14. K. B. K. Teo, M. Chhowalla, G. A. J. Amaratunga, W. I. Milne, G. Pirio, P. Legagneux, F. Wyczisk, J. Olivier, and D. Pribat, *J. Vac. Sci. Technol., B* **20**, 116 (2002).
15. S.-C. Seo and D. C. Ingram, *J. Vac. Sci. Technol. A,* **15**, 2579 (1997).
16. C. A. Spindt, I. Brodie, L. Humphrey, and E. R. Westerberg, *J. Appl. Phys.,* **47**, 5248 (1976).
17. I. Brodie and P. R. Schwoebel, *Proc. IEEE,* **82**, 1006 (1994).
18. Z. Xu, X. D. Bai, E. G. Wang, and Z. L. Wang, *Appl. Phys. Lett.,* **87**, 163106 (2005).